Low-q^2 Electron Scattering from the 15.109-MeV State of ^{12}C and the Conserved-Vector-Current Test*

B. T. Chertok and C. Sheffield
The American University, Washington, D.C. 20016

J. W. Lightbody, Jr., and S. Penner
National Bureau of Standards, Washington, D.C. 20234

D. Blum
Laboratoire de l'Accélérateur Linéaire, Orsay, France

(Received 27 December 1972)

High-precision electron scattering measurements from the 15.109-MeV 1^+ state in ^{12}C are made at $\theta = 75$ and $110°$ with $35 \leq E \leq 55$ MeV. From the measurements $B(M1)$ is extrapolated to the photon point and the radiative width is determined, $\Gamma_\gamma = 37.0 \pm 1.1$ eV. The corresponding weak magnetism results for β decay and μ capture are given.

I. INTRODUCTION

Transitions from the $T = 1$ isobaric state multiplet in the $A = 12$ system which corresponds to the ground states of ^{12}B and ^{12}N and the 15.109-MeV state of ^{12}C play an important role in physics encompassing aspects both of nuclear and particle physics.

Perhaps the most famous of these is the weak-magnetism test, which starting from the conserved-vector-current (CVC) theory, predicts that the electromagnetic matrix element for the 15.109-MeV decay in ^{12}C determines the strength of the weak matrix element in $^{12}B \overset{\beta^-}{\rightarrow} {}^{12}C$ and $^{12}N \overset{\beta^+}{\rightarrow} {}^{12}C$ for the $V-A$ interference.[1] The experimental observation of this effect in the β spectra of both ^{12}B and ^{12}N is confirmation of the CVC theory.[2] Moreover, the nonequality of ft values for this $T=1$ system poses a further interesting question – namely, is this nonequality due to currents omitted from the β-decay theory or due to nuclear dynamical effects? The high accuracy of the ft values and ratio $ft^+/ft^- = 1.103 \pm 0.009$ in the $A = 12$ system has led to an interest in second-class currents.[3] The resolution of this question should help to elucidate questions of great interest in nuclear physics, namely, charge independence violations and meson exchange currents in light nuclei.[4] Calculations of these phenomena have and will become more meaningful with improvement in the accuracy of the weak and electromagnetic transition matrix elements. The physical unity of weak and electromagnetic processes in this $A = 12$ system has been stressed recently and enlarged to include neutrino-induced reactions.[5]

The μ capture in ^{12}C leading to the ground state of ^{12}B, $\mu^- + {}^{12}C \rightarrow \nu_\mu + {}^{12}B$, since it proceeds via the analog of the $T = 1$, 15.109-MeV level provides independent testing of $\mu - e$ universality, weak magnetism,[6] or nuclear dynamics; probably nuclear dynamics, since at the present time the former are believed to be better understood.

The purpose of the experiment described in this paper is to make an accurate determination of Γ_γ and $B(M1, q^2)$ for low q^2 for the 15.109-MeV level in ^{12}C in order to increase the exactness of the weak magnetism tests primarily in β decay but also for μ capture.[7]

Table I displays the problem which we set out to resolve with the experiment reported here. Earlier measurements of the radiative width Γ_γ for the 15.109-MeV transition in ^{12}C have given an incompatible result, namely, $\Gamma_\gamma = 45.8 \pm 2.6$ eV[8] is the weighted average of six measurements using the technique of nuclear resonance fluorescence by several groups over a ten year period, while $\Gamma_\gamma = 32.6 \pm 3.5$ eV[7] is the result of combining three measurements from inelastic electron scattering. Consequently, a compilation value of $\Gamma_\gamma = 39.4$[8] which is a weighted average of $(\gamma, \gamma) + (e, e')$ data is suspect, as is its standard deviation of ± 1.5 eV, and the fit has a normalized $\chi^2 = 2.2$. A recent re-evaluation of the six resonance fluorescence measurements with currently accepted branching ratios yields a weighted average of $\Gamma_\gamma = 40.4 \pm 2.0$ eV.[9] In the compilation value, the (e, e') measurements did not include Coulomb corrections; however, the value reported above and in Table I, $\Gamma_\gamma = 32.6 \pm 3.5$ eV, does include these corrections. Any α-particle breakup of the 15.109-MeV state at the present level of accuracy[10] appears to be too small to be of significance here.

Inelastic electron scattering was used in the ex-

periment here to measure the transition probability $B(M1, q^2)$ connecting the ground and 15.109-MeV levels of ^{12}C. By measuring $B(M1, q^2)$ with good statistical accuracy for several values of q^2, the momentum transfer variable, near $q^2 = k^2$ an analytic relation between $B(M1, q^2)$ and q^2 is established, and this is extrapolated to give $B(M1)$ at the photon point. We will improve upon the results by adding electron scattering measurements of other laboratories which both overlap and extend our range of q^2. In so doing, one set of earlier measurements is not used although it displays a high degree of internal consistency[6]; it is about 20% lower in $B(M1, q^2)$[11] than the data from three other laboratories including the present one.

In Sec. II the experimental technique is described; in Sec. III the 11-parameter nonlinear least-squares fit to the measured electron spectrum is treated; in Sec. IV the reduction of the peak area ratio to the transition probability, $B(M1, q^2)$ is presented including a careful treatment, at the $\frac{1}{2}$ to 1% level, of kinematical and Coulomb distortion effects; this section concludes with the fitting of three trial functions to the data. In Sec. V our results are presented and used as inputs to determine precise values for the weak magnetism tests in $A = 12$ system. Appendix A gives a detailed treatment of the 11-parameter nonlinear least-squares fit to the spectra, and Appendix B summarizes the kinematical relations leading to the Jacobian of solid angles connecting the laboratory and c.m. frames.

II. EXPERIMENTAL TECHNIQUE

These measurements were made with the National Bureau of Standards (NBS) 150-MeV electron linac and 76-cm radius of curvature 169.8° double-focusing magnetic spectrometer. Scattered electrons were measured in a semiconductor detector ladder in the focal plane of the spectrometer and the beam current was measured with a Faraday cup. Details of the NBS electron scattering apparatus are described elsewhere.[12-14] The overall experimental resolution for this work was 0.1%. The data were taken at scattering angles of 75.2 and 110.64° with incident beam energies for these angles of 35.695, 40.638, 45.705, and 55.719 MeV at 75.2°, and 35.538, 40.599, 50.609, and 55.624 MeV at 110.64°. These kinematic conditions span a range of q^2 from 0.034 to 0.16 fm^{-2}.

Counts from the detector hodoscope were corrected for dead-time losses and accidental coincidences. Since in our detector system we make use of detectors which can move along the spectrometer focal plane we must properly include detector acceptance variation with position in the focal plane. This was done by normalizing the counts in a given detector to the counts which would have been received by that detector at a reference position in the focal plane. Relative detector efficiency corrections were then made to the counts from the various channels. The momentum interval subtended by each detector was computed based on spectrometer field setting, as well as detector position in the focal plane. Corrected counts from a given detector were then sorted into uniform momentum bins according to the detector overlap with the bin array. Bin widths chosen were 10 or 20 keV. The product of accumulated charge and detector momentum acceptance at the focal-plane reference position (mentioned above), corresponding to the counts in a given momentum bin, was stored in a separate array. Normalization to counts/(unit charge MeV/c) was then done by corresponding bin division. The spectra of counts/(unit charge MeV/c) were then fitted by analytic expressions and integrated in order to extract counts/unit charge corresponding to either elastic scattering or inelastic scattering to the 15.109-MeV state. This fitting procedure will be described in Sec. III.

Uncertainties in the experimental cross-section

TABLE I. Previous measurements Γ_γ (15.109 MeV) in ^{12}C (Table 12.8 in Ref. 8).

Method: (γ,γ) (eV)	Method: (e,e) (eV)
54.5 ± 9.3	40^{+8}_{-6}
59.2 ± 9.7	39 ± 4
40.2 ± 5.2	34.4 ± 3 [a]
54 ± 6	36.0 ± 3 [a]
50.5 ± 7.1	Orsay [a]
37 ± 5	
Weighted average 45.8 ± 2.6	32.6 ± 3.5 [b]

[a] Data used for least-squares fit in Ref. 7.

[b] Least-squares fit correcting each point for Coulomb effects (Ref. 7) (other entries in this column are not so corrected).

TABLE II. Peak area ratios.

E_i (MeV)	θ (deg)	q^2 (fm^{-2})	$10^4 A_i/A_e$	$\sigma(A_i/A_e)$ (%)
35.695	75.2	0.0338	0.850	6.54
40.638	75.2	0.0454	1.288	5.20
45.705	75.2	0.0591	1.632	4.42
55.719	75.2	0.0920	2.560	3.65
35.538	110.64	0.0560	3.516	4.73
40.599	110.64	0.0773	5.314	3.23
50.609	110.64	0.1298	8.151	2.72
55.624	110.64	0.1613	10.463	2.90

ratios given in Table II reflect uncertainties only due to counting statistics. To this uncertainty must be added 1% which we estimate is the possible systematic uncertainty due to beam misalignment on target, scattering-angle uncertainty, beam-energy uncertainty, target-thickness nonuniformity, current monitoring, and our ability to make the various counting-rate corrections. Since these are systematic effects we make a linear combination of this 1% with the statistical uncertainty.

The primary experimental objective of this research was to make accurate measurements of the ratio of two cross sections, $d\sigma/d\Omega$(15.109) and $d\sigma/d\Omega$ (elastic), as a function of momentum transfer. We employed a 22.1-mg/cm^2 graphite target which was oscillated in the electron beam so as to average over possible target nonuniformities. The area ratios were corrected for the small isotopic presence of ^{13}C. The 20-channel detector hodoscope located in the spectrometer focal plane was operated such that each detector made an independent cross-section measurement for the elastic and inelastic electron scattering. The relative detector efficiency therefore cancelled completely in analysis of cross-section ratios, with possible exceptions of multiple scattering effects which vary inversely with the final electron energy. We require that real electron scattering events have a signature made up of a triple coincidence between a single semiconductor detector and two large plastic scintillators which form a common backup function to all the semiconductor detectors. There is a finite probability that electrons which first pass through a semiconductor detector will be multiple scattered through sufficient angle such as not to pass through the scintillators, and therefore not be counted. For our lowest-energy electron scattering run, calculations indicate that the loss of efficiency due to this effect is less than 0.1% and therefore it was not considered in the data analysis.

Since the electron beam current is about a 100 times larger when measuring the inelastic—compared to elastic-peak regions, incident electron-beam charge-normalization effects also enter directly into the ratio measurement. In order to remove possible electrostatic charging effects in the Faraday-cup cooling system, the cooling water was drained from the cup. Later investigations have shown this to be essential for low current (several nanoamps average current) monitoring on the sub-one-percent level. Insofar as the separate charge measurements for each cross section were made over a broad range of incident beam currents, the Faraday-cup integrator calibration was essential.[14] A calibration of the integrator on different ranges was made with a precision current source and corrections were applied to the cross-section ratios; the corrections are accurate to 0.1%. Failure to capture the entire incident beam in the Faraday cup due to multiple scattering in the target is another effect which cancels in the ratio analysis.

III. DATA-ANALYSIS TECHNIQUES

The basic data consist of the total counts C_i falling within an energy range $(E_i - \Delta E,\ E_i + \Delta E)$, where $E_{i+1} - E_i = 2\Delta E$. At each incident energy and each scattering angle we have one sequence of counts spanning the elastic scattering peak and another sequence spanning the 15.109-MeV inelastic scattering peak. With $\Delta E = 5$ keV, there are approximately 100 discrete energy intervals $(E_i \pm \Delta E)$ and associated counts C_i to represent each peak. Since the standard deviation on each count is proportional to the square root of C_i, and since elastic scattering dominates strongly for the energies and angles used in this experiment, the statistical uncertainties reside mainly in the inelastic peak counts, to the point where the statistical uncertainty of the elastic peak counts has a negligible effect on the final results. The quantity used in calculating the $B(M1)$ transition probability for each incident energy and scattering angle is the ratio of the inelastic and elastic scattering peak areas, and the uncertainty in this ratio derives almost wholly from the statistical uncertain-

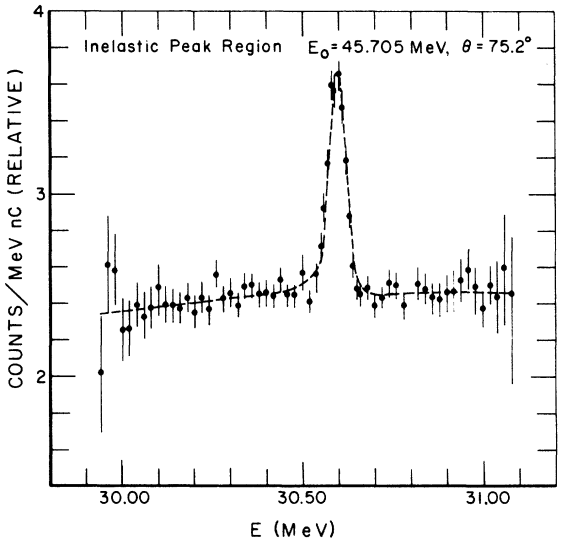

FIG. 1. The counts, associated standard deviations, and least-squares fit (dashed line) are displayed as a function of scattered electron energy for the inelastic peak region for the run at 75.2° and 45.705 MeV. The units of the ordinate are counts per MeV per nanocoulomb.

ty of the inelastic peak area. Figure 1 shows the counts and associated standard deviation bands for the inelastic peak for the run of 75.2° and 45.705-MeV incident electron energy.

Both the inelastic and elastic peaks have a substantial radiative tail, and the whole inelastic peak is superimposed on the tail of the elastic peak and must therefore somehow be separated from it before peak areas can be estimated. Such a separation can be performed, at least in part, by calculating a Schwinger correction to determine the fraction of electrons scattered from the peak to each part of the radiative tail. In practice, a better method is to give the tail a suitable parametric form, and determine the best values of the parameters via an over-all statistical fitting procedure, whereby the parameters of the inelastic peak are also determined. This was the method used here and described below.

The fitting of an 11-parameter model to the inelastic peak and radiative tail and the same model with two parameters constrained to zero for the elastic peak is described in detail in Appendix A. Figure 2 summarizes the fitting regions. 14 parameters are defined in Eqs. (A1), (A2), and (A3) and 11 free parameters a, b, c, α, E_{inel}, E_M, d, N_1, N_2, S_1, and S_2 remain after imposition of constraints. The method of least squares is used to determine the 11 parameters by first linearizing the highly nonlinear functional form for $C(E_i)$ and then iterating on the linearized least-squares fit.

Let C_i^{obs} be the observed count in the interval $(E_i - \Delta E,\ E_i + \Delta E)$ and C_i be the computed value for the set of 11 parameters $\vec{p} = p_j$ ($j = 1$ to 11). Then C_i depends on both E_i and $\vec{p}$, $C_i = C(E_i, \vec{p})$ and if W_i is the statistical weight associated with an observed value C_i^{obs}, we wish to determine $\vec{p}$ so as to minimize the residual sum of squares L,

$$L = \sum_{i=1}^{I} W_i [C_i^{\text{obs}} - C(E_i, \vec{p})]^2 , \tag{1}$$

where I is the total number of observed energy ranges (bins).

Since we iterate on $\vec{p}$, the minimization of L is with respect to $\Delta p_j = p_j - p_j^{(0)}$, where $p_j^{(0)}$ is any initial assumed set of parameters and it is assumed that $C(E_i, \vec{p})$ can be Taylor series expanded around $\vec{p}^{(0)}$ and linearized, see Eqs. (A5), (A6), and (A7). The solution to the linearized least-squares fit in matrix form is

$$\Delta \vec{p} = (A^T W A)^{-1} A^T W \Delta \vec{C} , \tag{2}$$

where

$$A_{ij} = \frac{\partial C(E_i, \vec{p})}{\partial p_j}\bigg|_{\vec{p}=\vec{p}^{(0)}} ,$$

$$\Delta \vec{C}_i = [C_i^{\text{obs}} - C(E_i, \vec{p}^{(0)})] ,$$

and

$$W_{ij} = W_i \delta_{ij} .$$

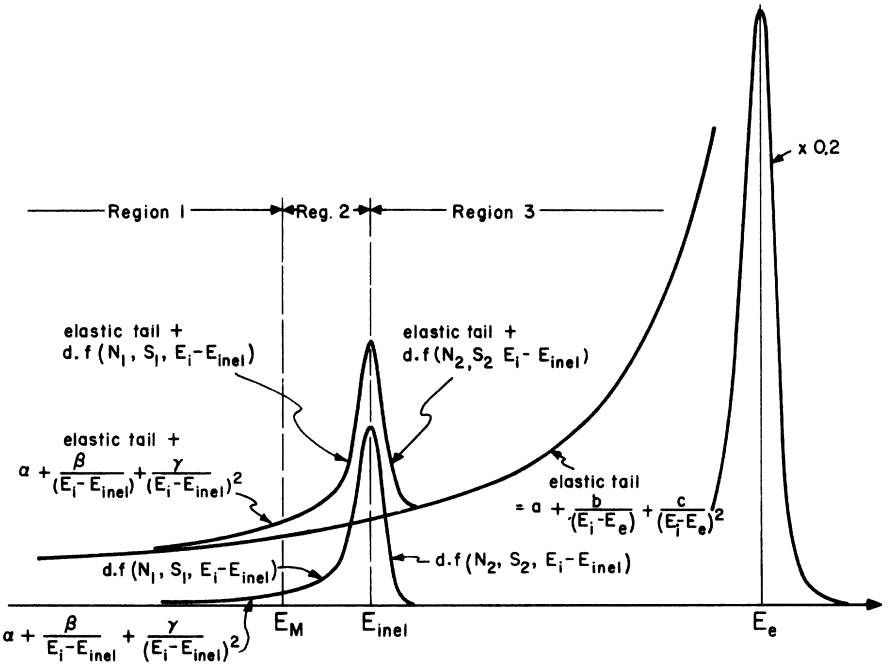

FIG. 2. The curves portray an idealized elastic peak, inelastic peak, and radiative tails as observed in electron scattering. The resulting spectrum is divided into three regions and is described by a 14-parameter model [see Eqs. (A1), (A2), and (A3)].

If the weights W_i are the reciprocal of the variances of C_i^{obs}, the matrix $(A^TWA)^{-1}$ is the variance-covariance matrix for the parameter set $\Delta\vec{p}$.

Thus a set of corrections $\Delta\vec{p}$ to $\vec{p}^{(0)}$ are determined to minimize L. If the neglected powers of $\Delta\vec{p}$ are not negligible, one iterates on $\vec{p}^{(1)}$, setting as a new initial vector

$$\vec{p}^{(1)} = \vec{p}^{(0)} + \Delta\vec{p} \tag{3}$$

until the new set $\Delta\vec{p}$ converges. In practice, three to six iterations sufficed to converge from an initial "eyeball" set $\vec{p}$ to a final set in which L changed by less than 10^{-6} on the last iteration. In Figure 1 the curve through the raw data is the final least-squares fit which required three iterations.

The physical quantity of interest is the area under the peak

$$A = \sum_{i=1}^{I} C(E_i, \vec{p}'), \tag{4}$$

where $\vec{p}'$ is the final vector of parameters but with the radiative tail removed, i.e., $a = b = c = 0$. The variance on A is given by

$$\mu(A) = [\sigma(A)]^2 = \sum_{i=1}^{I}\sum_{k=1}^{I} (A'B'A'^T)_{ik} \tag{5}$$

with $B = (A^TWA)^{-1}$. A' and B' are the matrices with rows and columns corresponding to the parameters a, b, and c deleted.

IV. CALCULATION OF $B(M1,q^2)$

A. Area Ratio and Jacobians

A functional fit of the type described in the preceding section was performed for both the elastic and inelastic peaks, for each incident energy and angle. From this analysis, peak areas and variances on peak areas were obtained. Since the graphite target contains ^{13}C with an isotopic abundance of 1.1% and ^{13}C is electroexcited by a $M1$ transition to a state at 15.1 MeV, the measured area ratios were increased by about 0.5% to yield the ^{12}C area ratios.[15] As mentioned earlier, the variance on the elastic peak area (A_e) is small compared with the variance on the inelastic peak area (A_{inel}), and the variance on the peak area ratios A_{inel}/A_e is thus essentially just the inelastic peak area variance. The ^{12}C peak area ratios, together with their corresponding standard deviations, are shown for each incident energy and scattering angle in Table II.

The transition probability $B(M1, q^2)$ is calculated using the ratio method,

$$\frac{A_{\text{inel}}}{A_e} = \frac{d\sigma_i/d\omega}{d\sigma_e/d\omega}, \tag{6}$$

where $d\sigma/d\omega$ are the cross sections in the laboratory coordinates (E_i, E_f, θ_e) which are first computed in the center-of-mass system with E_i', E_f', Θ and then transformed by the Jacobian of the solid angles J [Eq. (B6)], i.e.,

$$\left.\frac{d\sigma}{d\omega}\right|_{\text{lab}} = \left.\frac{d\sigma}{d\Omega}\right|_{\text{c.m.}} J . \tag{7}$$

The relevant expressions are given in Appendix B. The quantities $d\sigma_{\text{inel}}/d\Omega$ and $d\sigma_e/d\Omega$ are calculated using partial-wave analysis, the former in the distorted-wave Born approximation (DWBA) with

$$\frac{d\sigma_{\text{inel}}}{d\Omega} = \left.\frac{d\sigma_{\text{inel}}}{d\Omega}\right|_{\text{BA}} f_C \tag{8}$$

and the elastic scattering cross section without this approximation. The result for the $M1$ transition probability is

$$B(M1, q^2, \omega) = \frac{d\sigma_e}{d\Omega}\frac{J_e}{J_{\text{inel}}}\frac{A_{\text{inel}}}{A_e}\frac{9k_i'^2}{24\pi\alpha^2 q'^2 V_T'}\frac{1}{f_C}, \tag{9}$$

where k_i', q', and V_T' are computed in the c.m. system. These quantities are the incident electron momentum, three-vector momentum transfer, and kinematic parameter of transverse electroexcitation, respectively. The quantity f_C is the Coulomb-distortion correction to be discussed in the next section and α in Eq. (9), is the fine-structure constant. For the inelastic cross section, the results of Eq. (7) have been compared to an earlier calculation where k_i, q, and V_T are laboratory-system variables and a multiplicative factor $R^{-1} = [1 + (2E_i/M)\sin^2\frac{1}{2}\theta]$ is used to correct for recoil effects.[16] With a constant value for $B(M1)$ these cross sections differ by 0.34% at $E_i = 35.695$ MeV and $\theta = 75.2°$ and by 0.79% at $E_i = 55.624$ MeV and $\theta = 110.64°$, where $(d\sigma/d\omega)_i$ from Eq. (7) is larger than $(d\sigma/d\omega)_i$ computed directly in the laboratory system with recoil. At the present stage of inelastic electron scattering research at low q^2, these differences are submerged in larger statistical, instrumental, and unknown errors. However, measurements at the 1% level are becoming possible where the calculation embodied in Eq. (9) rather than one with recoil should be used. Appendix B contains a summary of the pertinent transformed variables.

We have computed the variation of $B(M1)$ over the ±1° angular spectrometer acceptance and found that the value of $B(M1)$ suitably averaged over the acceptance differs from the values at 75.2 and 110.64° by a negligible 0.04%.

B. Coulomb Corrections

Both the elastic and inelastic electron scattering cross sections are involved in the determination of $B(M1, q^2)$, since the area-ratio method is used. In Eq. (9), $(d\sigma/d\omega)_e$ and f_C are computed from partial-wave-analysis (PWA) programs. In earlier work $(d\sigma/d\omega)_e = \sigma_{\text{Mott}} F^2(q^2)$ and $f_C = 1.0$, which corresponded to treating ψ_i^e, ψ_f^e as plane waves. As has been pointed out,[17] the error in neglecting these Coulomb effects is magnified when $B(M1, q^2)$ is extrapolated to the photon point.

For $(d\sigma/d\Omega)_e$ we have used the PWA computer calculation of Rawitscher and Fischer which includes double-precision arithmetic and c.m. corrections due to Bergstrom and Ziegler.[18] Both harmonic-oscillator and Fermi charge distributions from a recent high-accuracy elastic electron scattering measurement[19] of ^{12}C were used to compute the cross section where

$$R_{\text{HO}} = 2.453 \pm 0.008 \text{ fm}, \quad a = 1.687, \quad \alpha = 1.067$$

and

$$R_{\text{F}} = 2.445 \pm 0.015 \text{ fm}, \quad c = 2.56 \text{ fm}, \quad t = 1.69 \text{ fm}.$$

For our eight data points plus the eight points from Yale[18] and Orsay,[20] the maximum difference in the computed $(d\sigma/d\Omega)_e$ using ρ_{HO} and ρ_{F} is less than 0.2%. Thus the elastic cross section is sensitive only to R_m, the rms charge radius of ^{12}C in the present range of q^2. The harmonic-oscillator values have been used, since higher q^2 measurements select ρ_{HO} over other ground-state charge distributions.

TABLE III. Input data for fitting.

q^2 (fm^{-2})	$B(M1, q, \downarrow)$ (10^{-2} fm^2)	$[\sigma(B(M1))]^{-2}$ [a]
0.0338	0.9076	213
0.0454	0.9737	275
0.0591	0.9024	419
0.0920	0.8290	674
0.0560	0.8191	454
0.0773	0.8449	785
0.1298	0.6777	1570
0.1613	0.6505	1558
0.1295 [b]	0.6854	213
0.2730	0.4571	479
0.1185 [c]	0.728	385
0.1519	0.667	459
0.1880	0.519	758
0.1894	0.593	1138
0.2310	0.527	1441
0.2768	0.452	3058

[a] 1% has been added *linearly* to the σ in Table II and to the data of Ref. 15.

[b] 0.1295 + 0.2730 are from Ref. 20.

[c] 0.1185 to 0.2768 inclusive are from Ref. 15.

In the case of Coulomb corrections for the inelastic cross section, it has been pointed out that a consistent determination of f_C requires knowledge of a nuclear model through exact determination of $B(M1)$ vs q^2; the Coulomb-distortion parameter $f_C = d\sigma(\text{DWBA})/d\sigma(\text{PWBA})$ is fully described elsewhere.[7] Since both f_C and $B(M1)$ are linearly proportional to the measured $(d\sigma/d\Omega)_{\text{inel}}$, an iteration is required. Furthermore, it has been pointed out by Drechsel[21] that the expansion coefficients for transverse electroexcitation, e.g. in $B(M1, q^2) = a + bq^2 + cq^4 \cdots$ have interpretations which are also model-dependent. Thus if b is interpreted as the square of a transition radius, $b \propto R_{\text{tr}}^2$, then R_{tr} is not invariant but a strong function of the model.

This problem is avoided here by checking the sensitivity of f_C within one model to rather large variations in the parameters. Specifically an incompressible irrotational liquid-drop model is used for the transition current distribution $\vec{J}_N = \rho(M1)\vec{Y}^M_{L,L,1}$, where

$$\rho(M1) = \frac{d\rho_0}{dr} \tag{10}$$

and ρ_0 is the Fermi distribution. As noted earlier (i.e., Fig. 1 of Ref. 7) for the kinematic variables used here, f_C is insensitive to large variations in $\rho(M1)$. The quantity f_C has been computed with the quoted ground-state Fermi parameters, $c = 2.56$, $t = 1.69$. The average deviation of f_C with respect to c, t for fixed ground-state radius over the set of 16 data points (8 NBS, 2 Orsay, and 6 Yale) is

$$\frac{\overline{\Delta f}}{f} \lesssim 0.1\%,$$

where $\rho(c = 2.56, t = 1.69)$ is compared with $\rho(c = 1.79, t = 2.40)$. The largest individual deviation is 0.4%. The average deviation over the same data set for a 12% increase in radius, i.e., for $R_m = 2.45$ and $R_m = 2.74$ fm, is

$$\frac{\overline{\Delta f}}{f} = 0.3\%.$$

The largest individual deviation is 2.1% for the point at $q^2 = 0.273$ fm^{-2}. Thus we are satisfied with the insensitivity of f_C to the model and parameters (same as the ground state of ^{12}C) that have been used in the calculation.[22] It is to be stressed that confidence in the accuracy of f_C is based here on: (1) the data set being restricted to low q^2 and relatively small angles and (2) on a low-Z nucleus such as $^{12}_{6}$C; i.e., compare Figs. 1 and 2 of Ref. 7.

Finally then these variables are combined in Eq. (9) to compute $B(M1, q^2, \downarrow)$ where $\downarrow$ stands for the downward $1^+ \rightarrow 0^+$ transition. The results are

given in Table III. In this table the results of the present reanalysis of the Orsay data[20] (2 points) and Yale data[15] (6 points) are included, i.e., both sets of measurements were reported before reliable partial-wave analyses of elastic and inelastic electron cross sections were available. The former were analyzed from the referenced area ratios by Eq. (9). For the latter data set, the $B(M1)$'s were scaled with Coulomb corrections for both elastic and inelastic scattering and to the new ground-state radius of 2.453 fm. This resulted in a $B(M1)$ reduction of each of the Yale points uniformly by about 10%. The weights in Table III are computed by first adding 1% *linearly* to the standard deviations of the area ratios in Table III, i.e., $\sigma = \sigma(A_{\text{inel}}/A_e) + 1\%$. As described in Sec. II this represents an estimate of the lack of understanding of experimental effects which contribute to the area ratios which have been deduced from the measurements. The same 1% estimated error has been added linearly to the uncertainties reported on the set of Yale points to reflect an estimate of the true uncertainty after our reanalysis of that data. That this analysis of the total standard deviation on $B(M1)$ is conservative, is observed in the next section where the fitted function of the set of $B(M1)$ vs q^2 has a $\chi^2 = 0.74$ per degree of freedom.

C. Fitting of $B(M1, q^2)$

To describe $B(M1, q^2)$ as a function of q^2 for extrapolation to the photon point, three functional forms (models) were used and fitted for a_1, a_2, a_3, or $B(M1, 0)$ and b using least squares:

$$\text{(a) } B(M1, q^2) = a_1 + a_2(q^2 - k^2),$$

$$\text{(b) } B(M1, q^2) = a_1 + a_2(q^2 - k^2) + a_3(q^4 - k^4), \quad (11)$$

$$\text{(c) } B(M1, q^2) = B(M1, 0)(1 - \tfrac{1}{6}\eta^2 + \tfrac{1}{8}\rho\eta^2)^2 e^{-\eta^2/2},$$

where k is the photon wave number, $\eta = qb$ and b is the oscillator parameter, and $\rho = 0.23 \pm 10\%$.[23] The least-squares fit is clearly linear for (a) and (b) and nonlinear for (c),[5,6] the latter function being fitted in this work by an iteration procedure known as parabolic extrapolation of χ^2.[24]

Of the three fitting functions used only Eq. (11c) is explicitly based on a nuclear model. Kurath[25] has shown that for $1p$ shell nuclei, magnetic dipole transitions can be described by

$$B(M1, q) = B(M1, 0)[\langle j_0 \rangle + \rho\langle j_2 \rangle]^2, \quad (12)$$

where $B(M1, 0)$ and ρ are functions of the spin-orbit coupling and $\langle j_L \rangle$ is the radial integral

$$\langle j_L \rangle = \int_0^\infty R_{1p}^2(r) j_L(qr) r^2 \, dr. \quad (13)$$

It is now known that ρ is near the LS limit in ^{12}C with a value $\rho = 0.23 \pm 10\%$. The reduced nuclear transition probability in Eq. (11c) results from evaluating (13) with a harmonic-oscillator radial wave function, $R_{1p} = N_{1p} r e^{-1/2(r/b)^2}$.

The variance-covariance matrix for these fits was computed, also a normalized χ^2 defined by

$$\chi^2 = \sum_{i=1}^{N} \frac{[B_E(i) - B_c(i)]^2}{\sigma_i^2 \nu}, \quad (14)$$

where N represents number of data points; ν represents degrees of freedom and is equal to N minus the number of parameters in fitting function; $B_E(i)$ is the experimental value of $B(M1, q^2)$ at ith data point; $B_c(i)$ is the computed value of

TABLE IV. Fits to $B(M1)$ versus q^2.

Data	Fit [a]	Γ_γ (eV)	σ_{Γ_γ} (eV)	ν [b]	χ^2
NBS	$N=2$	36.18 ± 1.24		6	0.88
NBS	$N=3$	37.43 ± 3.06		5	1.00
NBS	$1p$ oscillator [c]	37.33 ± 1.65		6	1.00
ALL	$N=2$	34.35 ± 0.76		14	1.02
ALL	$N=3$	37.48 ± 1.53		13	0.70
ALL	$1p$ oscillator [d]	36.95 ± 1.08		14	0.74

[a] Equations (11a), (b), and (c) for $N=2$, $N=3$, and $1p$ oscillator, respectively.
[b] ν is degrees of freedom.
[c] $b_{\text{osc}} = 1.905 \pm 0.121$ fm.
[d] $b_{\text{osc}} = 1.881 \pm 0.053$ fm.

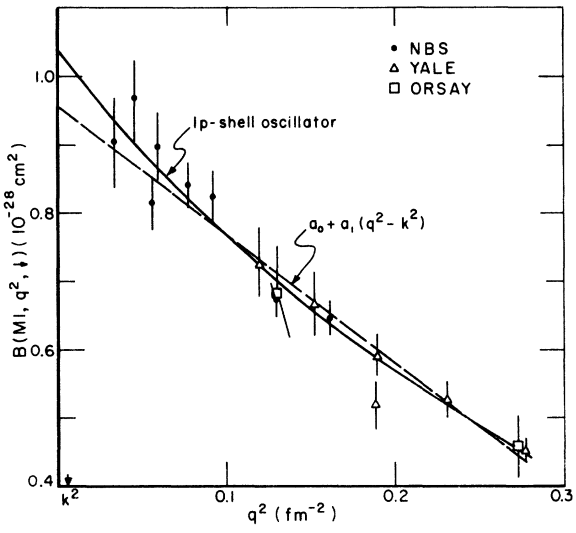

FIG. 3. Fits using Eq. (11) are presented to the experimental reduced nuclear transition probability versus momentum transfer squared. The data from Yale (Ref. 15) and Orsay (Ref. 20) as reanalyzed here are included with our measurements.

$B(M1, q^2)$ using a_1, a_2, a_3, or $B(M1, 0)$ and b from least-squares fit.

The results of fits to the data set are given in Table IV where the fit $N=2$ uses Eq. (11a), $N=3$ uses Eq. (11b), and the $1p$ oscillator uses Eq. (11c). The data points and two of the fits are displayed in Fig. 3. For the National Bureau of Standards measurements alone (8 data points), the χ^2 as reported in Table IV indicates a good fit to the three models. When the Orsay and Yale data are added, thereby increasing the data set from 8 to 16 points (ALL) they provide a higher q^2 anchor for the various fits. One observes that the photon points (and value of b) have not changed for $N=3$ and $1p$ oscillator models in enlarging the data set but that the corresponding χ^2 have decreased from 1.0 to 0.7, indicating an underestimate of the weights $1/\sigma_i^2$ for the data set. To verify this point the results in Table IV were generated for the input data with 1% added in *quadrature* rather than *linearly* as in Table III. With these weights the χ^2 for the six rows in Table IV are 1.31, 1.46, 1.48, 1.44, 0.98, and 1.03, respectively, which is indicative of substantially better fit to the set of 16 rather than 8 data points and then preferentially for only the $N=3$ or $1p$-shell oscillator models. By substantially better one means the probability $P(\chi^2, \nu)$ of exceeding χ^2 is much larger, i.e., $P(1.0, 14)=0.42$ versus $P(1.5, 14)=0.10$. The photon point values are unchanged and their uncertainties only altered moderately with the larger weights. However, we prefer the smaller weights from $\sigma=\sigma_{\text{exp}}+1\%$ as a better measure of uncertainties both in the experiment and reanalysis of Yale and Orsay data.

The $1p$-shell harmonic-oscillator fit is selected for two reasons:

(1) The linear fit in q^2 ($N=2$) for ALL is an improbable fit to the subset of the 8 NBS points at low q^2 giving a $\chi^2=1.42$ with 4 of 8 data points falling $\gtrsim\sigma$ outside this fit (see Fig. 3), whereas the $1p$ oscillator model has a χ^2 for this same subset of 1.02 missing 2 of 8 data points at the one σ level.

(2) More importantly analysis of experimental data for the electroexcitation of the 15.109-MeV state up to much larger $q^2\simeq 2$ fm^{-2} indicates that the $1p$-shell oscillator model [Eq. (11c) of this section] which results from a straightforward calculation of the spin-isospin flip $1p_{3/2}^{-1}1p_{1/2}$ component in ^{12}C gives a reasonable fit to the data subject only to a normalization factor of 4 in the $B(M1, q^2)$.

The normalization problem appears to be understood.[5] It is estimated that the $N=2$ fit would fall below the experimental data at $q^2\approx 0.4$ fm^{-2} by factors of 3–5.[5, 6, 26]

V. RESULTS

The radiative width is determined by extrapolation of a fitting function to the photon point ($q^2=0.005\,86$ fm^{-2}). The fit to the combined NBS, Yale, and Orsay data using a $1p$-shell oscillator model is believed to be the best over-all fit with $B(M1, 0, \downarrow)=0.010\,40\pm0.000\,29$ fm^2 and $b=1.881\pm0.053$ fm.

The radiative width of the 15.109-MeV state of ^{12}C as determined by inelastic electron scattering is

$$\Gamma_\gamma=37.0\pm1.1\text{ eV},$$

where the quoted uncertainty is the standard deviation. This result is in excellent agreement with the most recent (γ, γ) measurement of 37 ± 5 eV.[27]

From the best fit of the combined data, the ratio of the $B(M1)$'s for the μ capture to β-decay reactions at $q^2=0.216$ and 0 fm^{-2}, respectively, is determined. This result is

$$\frac{B(M1, q^2=0.216)}{B(M1, 0)}=0.555\pm0.019$$

with the oscillator parameter

$$b=1.88\pm0.05\text{ fm},$$

which compares very well with 1.92 ± 0.03 fm from Eq. (25) of Ref. 6. Thus the shape of the earlier $B(M1)$ versus q^2 from electron scattering data as analyzed in Ref. 6 from the data of Ref. 11 is in agreement with ours even though the magnitude was about 11% lower. The disagreement in magnitude is enlarged to about 20% when Coulomb distortion corrections are included which accounts for the value $\Gamma_\gamma=32.6\pm3.5$ eV reported earlier.[7] The discrepancy is not due to any Coulomb distortion corrections which we estimated to have an uncertainty of about 1%. Hence as mentioned in the Introduction, that data set consisting of 14 points is excluded here. The earlier value of the $B(M1)$ ratio is 0.53 ± 0.02; the identical uncertainties are accidental, resulting from compensating errors in b and ρ for the $1p$ oscillator fit. For completeness the variance-covariance matrix for the two-parameter fit to Eq. (11c) is given:

$$\begin{pmatrix} 8.663\times10^{-8} & -1.572\times10^{-5} \\ -1.572\times10^{-5} & 2.852\times10^{-3} \end{pmatrix}.$$

The parameter vector is

$$\begin{pmatrix} B(M1, 0) \\ b \end{pmatrix}.$$

It is to be noted that the value of the oscillator parameter $b=1.77$ fm which has been used in recent work[5,26] gives a comparatively unacceptable

fit to the present low-q^2 data in yielding a normalized $\chi^2 = 1.46$. The effect on their results of using $b = 1.88$ fm appears to be small.

The new values of Γ_γ and the $B(M1)$ ratio with a substantially reduced uncertainty for the radiative width can be applied to the weak magnetism tests. For the comparison of β-decay matrix elements from ^{12}B ($T_3 = +1$), ^{12}C ($T_3 = 0$), and ^{12}N ($T_3 = -1$), the shape correction factors $S^{\pm}(E) = 1 + a^{\pm}E$ can be: (1) measured in β decay as deviations from allowed shapes in the Kurie plots[2] or (2) predicted from the conserved-vector-current theory.[1] The prediction is

$$a^{\pm} = \mp \frac{8}{3}\left(\frac{3\Gamma_\gamma f t^{\pm}}{4\alpha\omega_0^3 f t_F}\right)^{1/2} \pm \frac{24}{15} Z\alpha R, \tag{15}$$

where a^+ refers to ^{12}N (β^+) and a^- to the ^{12}B (β^-) β decay. The second term in Eq. (15) is a Coulomb correction in β decay[28] which is included in the experimental values of a^+ and a^-. The uncertainty in this correction term which is dominated by the nuclear model dependency is taken into account and is conservatively 20%.[29] R is the equivalent uniform charge distribution radius which is $(\frac{5}{3})^{1/2}$ larger than the rms radius determined by elastic electron scattering. At the present level of accuracy of the ft and Γ_γ values, it is meaningful to distinguish between a^+ and a^- slopes. That is, we dispense with the older use of

$$\frac{S(\beta^-)}{S(\beta^+)} = 1 + (A + \delta A)E,$$

where

$$A = \frac{1 + a^-}{1 + a^+} \simeq 1 + 2|a^-|,$$

since $a^- \neq a^+$ and this difference as evidenced by the current discussion of second-class currents, meson exchange, and nuclear dynamics is of significant interest. Instead, the individual $V-A$ interference terms a^- and a^+ are reported here with $S = 1 + aE$ and then compared with experiment. a^- and a^+ are defined in Eq. (15) to include separate Coulomb corrections for β^- and β^+ which were formerly included in δA above.[28] The ft values for the universal vector transition and β^- and β^+ legs of the $A = 12$ nuclei are undergoing continuous refinements. Nevertheless, a set ft_F, ft^-, and ft^+ are determined from the current literature as given below.

TABLE V. β,γ weak-magnetism test in $A = 12$.

	a^+ (MeV^{-1})	a^- (MeV^{-1})
Experiment:		
wide slits	$(-0.50 \pm 0.09) \times 10^{-2}$	$(+0.52 \pm 0.09) \times 10^{-2}$
narrow slits	$(-0.52 \pm 0.06) \times 10^{-2}$	$(+0.55 \pm 0.10) \times 10^{-2}$
Theory:		
Eq. (15)	$(-0.466 \pm 0.024) \times 10^{-2}$	$(+0.438 \pm 0.024) \times 10^{-2}$

For the calculation, we use

$$ft_F = ft_{^{14}\mathrm{O}} = 3094 \pm 12 \text{ sec},^{30}$$

$$ft^- = ft_{^{12}\mathrm{B}} = 11\,962 \pm 48 \text{ sec},$$

$$ft^+ = ft_{^{12}\mathrm{N}} = 13\,194 \pm 92 \text{ sec},$$

$$\omega_0 = 15.109 \pm 0.004 \text{ MeV},$$

$$\Gamma_\gamma = 37.0 \pm 1.1 \text{ eV}.$$

The values of $ft^{\pm}$ are computed using literature values of end-point energies,[31] half-lives,[3] branching ratios,[3] radiative corrections,[32] and f values.[31] The errors are propagated independently. Since the reported end-point energy of ^{12}N has decreased to $W_0 = 16.831 \pm 0.005$ MeV[3] from the value used earlier, 16.838 ± 0.005 MeV,[31] and thereby affects f, we have computed the ft^+ by normalizing to Wilkinson's value for the $A = 12$ ratio $ft^+/ft^- = 1.103 \pm 0.009$.[3]

The values of $a^{\pm}$ for experiment[2] and theory are presented in Table V. The agreement as in the past is clearly good.[33] The error in the Coulomb correction dominates the total error in a, which is now ±5%; the error in Γ_γ is almost a factor of 5 smaller than the previous best measurement,[27] which in our judgment, was $\Gamma_\gamma = 37 \pm 5$ eV and results in a ±1.5% uncertainty in the first term in Eq. (15). With the tightened constraints further more precise measurements of either a^+ or a^- from β spectra would appear to be quite meaningful.

For the second test of weak magnetism in the $A = 12$ system proposed by Foldy and Walecka the dominant matrix element in the μ-capture reaction

$$\mu^- + {}^{12}\mathrm{C} \rightarrow \nu + {}^{12}\mathrm{B}$$

is related in an essentially model-independent way to experimental ft value for

$${}^{12}\mathrm{B} \rightarrow e^- + \bar{\nu} + {}^{12}\mathrm{C}$$

and to the ratio $B(M1, q^2)_{\mu \text{ capture}}/B(M1, 0)_{\beta \text{ decay}}$ determined by inelastic electron scattering from the 15.109-MeV state of ^{12}C.[6] This dominant part (about 68%) of the μ-capture rate is

$$\frac{\nu^2\mu^3}{2\pi^2}|GF_A^{\beta}|^2 \sum_{M_f}\left|\int \sigma\right|^2 = \frac{3\pi\nu^2 m_\mu{}^3 \ln 2}{m_e{}^5 f t_{^{12}\mathrm{B}}} \times \frac{B(M1, q^2 = 0.216)}{B(M1, 0)} C, \tag{16}$$

where C, a correction to the axial-vector transition for second-forbidden transitions, is

$$C=\left(\frac{1-\frac{1}{6}\eta^2}{1-\frac{1}{6}\eta^2+\frac{1}{6}\rho\eta^2}\right)^2, \tag{17}$$

where $\rho=0.23\pm10\%$,[23] $\eta=bq$, and b is the oscillator parameter. The energy transfer is $\nu=91.67$ MeV. The symbols appearing in Eq. (16) are as defined in Ref. 6.

Using the values of the $B(M1, q^2)$ ratio and b determined in the present work together with $ft_{^{12}\mathrm{B}}=11\,962\pm48$ sec, we calculate

$$\frac{\nu^2 m_\mu{}^3}{2\pi^2}\,|GF_A^\beta|^2\sum_{M_f}\left|\int\vec{\sigma}\right|^2=8.07\pm0.31\times10^7\ \mathrm{sec}^{-1},$$

where the errors in Eq. (16) are taken to be correlated for the product $[B(M1, q^2)/B(M1, 0)]C$. This compares with the published value, Eq. (32) of Ref. 6 of $8.08\times10^7\ \mathrm{sec}^{-1}\pm5\%$.

From the correction C in Eq. (17), the second-forbidden contribution to the axial-vector matrix element is determined from $1-\sqrt{C}$ to be $3.3\pm0.4\%$. We do not proceed to a direct comparison of this new result with CVC, since the analysis is rather involved and beyond the scope of the present work.[5,6] Suffice it to comment that the dominant part for the μ-capture reaction, Eq. (14) has been determined to $\pm3.8\%$.[34] Increased accuracy in measurements of the μ-capture rate on ^{12}C together with a reduction in the uncertainty on the oscillator parameter b would considerably tighten this test.

We summarize the results of this experiment and analysis of electron scattering from the 15.109-MeV level of ^{12}C. Figure 4 summarizes the relevant dynamics in the $A=12$ system.

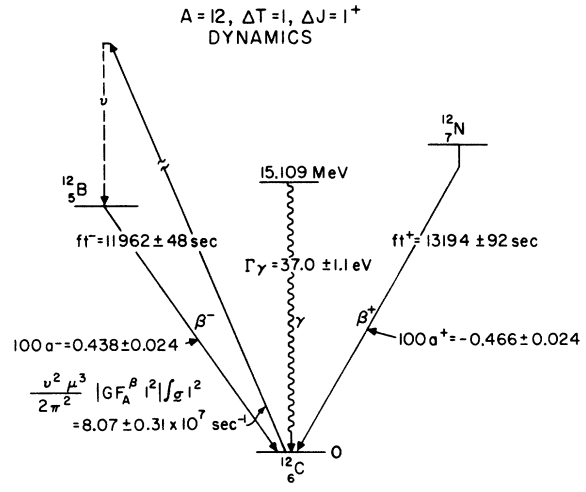

FIG. 4. The electromagnetic and weak transitions of the $A=12$, $T=1$ system are displayed on this energy level diagram and include the weak magnetism results of the present experiment and analysis.

(1) 16 data points span q^2 from 0.034 to 0.277 fm^{-2} and are fitted well with a normalized $\chi^2=0.74$ by the $1p$-shell oscillator fit [see Eq. (12)],

$$B(M1, q^2)=B(M1, 0)\left[1-\frac{(1-\rho)}{6}\eta^2\right]^2 e^{-\eta^2/2}$$

with $B(M1, 0, \text{⬍})=0.010\,40\pm0.000\,29$ fm^2, $b=1.881\pm0.053$ fm ($\eta=bq$), and $\rho=0.23\pm10\%$ which yield at $q^2=k^2$ a radiative width

$$\Gamma_\gamma=37.0\pm1.1\ \mathrm{eV}.$$

(2) The radiative width and $B(M1, q^2)$ ratio are applied to the CVC weak magnetism predictions in the $A=12$ system and yield tests of the β-decay effect at the 5% one σ level (where over three quarters of this uncertainty comes from the Coulomb corrections to β decay) and give the dominant part of the μ-capture rate in ^{12}C to 3.8%. This results, respectively, in a fourfold and 30% reduction compared to previous work[6,27] in the uncertainties of the basic electromagnetic parameters used in the weak magnetism tests.

(3) An 11-parameter model is described and used in an iterated least-squares fit to extract areas ratios and variances from electron scattering spectra which obviates the determination and removal of radiative effects from the inelastic and elastic peak areas.

(4) Coulomb distortion corrections and kinematical effects are treated carefully in the low-q^2 region to reduce uncertainties from these sources to $\lesssim1\%$ in the determination of the reduced nuclear transition probabilities.

(5) Finally a comparison of our low-q^2 electron scattering results with photon absorption from the 15.109-MeV state indicates agreement in radiative widths at the 10% level, 37.0 ± 1.1 eV and 40.4 ± 2.0 eV,[9] respectively. After the present publication was in preparation, we learned that an Amsterdam-Darmstadt collaboration has measured the 15.109-MeV ^{12}C form factor in the range $0.04<q^2<0.44$ fm^{-2} and they report $\Gamma_\gamma=35.74\pm0.86$ eV and $b=1.882\pm0.021$ fm.[35] One can conclude that there is agreement at the 3% level of accuracy on the 15.109-MeV level ^{12}C electron scattering cross section at low momentum transfer among all recent experiments (the present work, the Amsterdam-Darmstadt collaboration mentioned above, and the Yale results of Ref. 15). It is our belief that the measurements reported in Ref. 11 are in error by about 20% and should not be used. It is perhaps worth reiterating that accurate extrapolation to the photon point requires that the electron scattering data span a broad range of momentum transfer, that Coulomb dis-

tortion corrections be carefully applied even for low-Z nuclei, and that an appropriate (nonlinear) extrapolating function be used. In conclusion, we believe that the 15.109-MeV ^{12}C level form factor can be used as a bench mark for low-q^2 measurements of nuclear excited-state cross sections.

APPENDIX A

An 11-parameter model was used as a functional form for the inelastic peak and radiative tail, and the same model with two parameters constrained to zero was used on the elastic peak. For the inelastic peak, as displayed in Fig. 2, the model has the form:

Region I: Energy $\equiv E_i < E_M \equiv$ matching energy.

Count in energy range $(E_i - \Delta E,\ E_i + \Delta E)$

$$\equiv C(E_i) = a + b(E_i - E_e)^{-1} + c(E_i - E_e)^{-2} + \alpha + \beta(E_i - E_{\text{inel}})^{-1} + \gamma(E_i - E_{\text{inel}})^{-2}, \tag{A1}$$

where E_e is the energy of the elastic peak maximum and E_{inel} is the energy of the inelastic peak maximum.

Region II: $E_M \leq E_i < E_{\text{inel}}$.

$$C(E_i) = a + b(E_i - E_e)^{-1} + c(E_i - E_e)^{-2} + df(N_1, S_1, E_i - E_{\text{inel}}), \tag{A2}$$

where $f(N, S, E) = [1 + 4E^2(2^{1/N} - 1)/S^2]^{-N}$.

The function $f(N, S, E)$ tends to a Gaussian distribution as $N \to \infty$, and for small values of N it has a tail that decreases less rapidly than a Gaussian as E increases.

Region III: $E_{\text{inel}} \leq E_i$.

$$C(E_i) = a + b(E_i - E_e)^{-1} + c(E_i - E_e)^{-2} + df(N_2, S_2, E_i - E_{\text{inel}}). \tag{A3}$$

The main points about the above functional forms are:

(a) In each region there is a radiative tail from the elastic peak. (See Fig. 2.)

(b) In Region I there is also a radiative tail from the inelastic peak.

(c) In Regions II and III forms similar to Gaussians are superimposed on the elastic radiative tail. The parameters S_1 and S_2 are analogous to the width σ of a Gaussian distribution, thus different peak half-widths are permitted above and below the energy of the inelastic peak maximum.

From the above functional forms, we see that there are 14 parameters to be determined, viz., a, b, c, α, β, γ, E_e, E_{inel}, E_M, d, N_1, N_2, S_1, and S_2. However, the elastic peak energy is well known, and the results are in any case very insensitive to its value. Thus, E_e is not used as a parameter. In addition, we wish the over-all peak to be a continuous function of E and to have a continuous first derivative at $E = E_M$. Applying these constraints to determine β and γ in terms of the other parameters leaves us with an 11-parameter model in terms of a, b, c, α, E_{inel}, E_M, d, N_1, N_2, S_1, and S_2. The general technique we will use to determine these 11 parameters from the given counts C_i is the well-known method of least squares. However, because the functional form for $C(E_i)$ is highly nonlinear in several of the parameters an iterated linearized least-squares procedure must be adopted. Before describing this, let us remark that we also have a model for the elastic peak if we require that $b = c = 0$ and replace E_{inel} by E_e in the above discussion. The nine parameters for the elastic peak are thus a, α, E_e, E_M, d, N_1, N_2, S_1, and S_2. With this understanding, all subsequent remarks on fitting procedures apply equally to the inelastic or the elastic peak.

Linearized Least-Squares Fitting Procedure

Let C_i^{obs} be the observed count in the energy range $(E_i - \Delta E,\ E_i + \Delta E)$, and let $C_i \equiv C(E_i)$ be the computed value in the same energy range for any set of values of the 11 parameters. Let the parameters be denoted by $\vec{p} \equiv p_j$ ($j = 1$ to 11), and let $\vec{p}^{(0)}$ by any initial assumed set of values of p_j. Then C_i depends on both E_i and $\vec{p}$, $C_i = C(E_i, \vec{p})$, and if W_i is the statistical weight associated with an observed value C_i^{obs}, we wish to determine a set $\vec{p}$ that minimizes the weighted sum of squares of residuals L:

$$L = \sum_{i=1}^{I} W_i (C_i^{\text{obs}} - C(E_i, \vec{p}))^2, \tag{A4}$$

where I is the total number of observed energy ranges. Expanding $C(E_i, \vec{p})$ about $p_j^{(0)}$,

$$C(E_i, \vec{p}) = C(E_i, \vec{p}^{(0)}) + \sum_{j=1}^{11} \left(\frac{\partial C(E_i, \vec{p})}{\partial p_j} \bigg|_{\vec{p} = \vec{p}^{(0)}} \right) (p_j - p_j^{(0)}) + O([p_j - p_j^{(0)}]^2). \tag{A5}$$

Writing $p_j - p_j^{(0)} = \Delta p_j$, $C_i^{\text{obs}} - C(E_i, \vec{p}^{(0)}) = \Delta C_i$, and dropping all except the linear terms in Δp_j in the expan-

sion, we have

$$L=\sum_{i=1}^{I} W_i \left(\Delta C_i - \sum_{j=1}^{11} \frac{\partial C(E_i,\vec{p})}{\partial p_j}\bigg|_{\vec{p}=\vec{p}^{(0)}} \Delta p_j\right)^2 . \tag{A6}$$

Minimizing L with respect to Δp_k, we require $\partial L/\partial \Delta p_k = 0$:

$$\frac{\partial L}{\partial \Delta p_k} = -2 \sum_{i=1}^{I} \frac{\partial C}{\partial p_k}(E_i,\vec{p})\bigg|_{\vec{p}=\vec{p}^{(0)}} \cdot W_i \cdot \left(\Delta C_i - \sum_{j=1}^{11} \frac{\partial C(E_i,\vec{p})}{\partial p_j}\bigg|_{\vec{p}=\vec{p}^{(0)}} \cdot \Delta p_j\right) = 0 . \tag{A7}$$

Now we define matrices W and A, where $(W)_{ij} = W_i \delta_{ij}$, $(A)_{ij} = \partial C(E_i,\vec{p})/\partial p_j \,|_{\vec{p}=\vec{p}^{(0)}}$ and vectors $\Delta\vec{C}$, $\Delta\vec{p}$, where $(\Delta C)_i = \Delta C_i$, $(\Delta p)_j = \Delta p_j$. The set of Eqs. (7) can then be written in compact form

$$(A^T W A)\Delta\vec{p} = A^T W \Delta\vec{C} \tag{A8}$$

with the immediate solution

$$\Delta\vec{p} = (A^T W A)^{-1} A^T W \Delta\vec{C} . \tag{A9}$$

Thus, subject to the validity of dropping higher powers of Δp_j from the expansion (A5), we have determined a set of corrections $\Delta\vec{p}$ to the assumed set $\vec{p}^{(0)}$ so as to minimize L. However, if the neglected powers of $\Delta\vec{p}$ are not negligible, it will be necessary to form a new initial vector $\vec{p}^{(1)} = \vec{p}^{(0)} + \Delta\vec{p}$, to replace $\vec{p}^{(0)}$ by $\vec{p}^{(1)}$, and to repeat the calculation for a new set $\Delta\vec{p}$. This procedure is repeated until further iteration produces no change in L, at which point a best value of the parameters $\vec{p}$ consistent with the data and the chosen model has been found. Several comments are in order regarding this procedure:

(a) In order that $(A^T W A)$ be nonsingular, the number of observations must be at least equal to the number of parameters.

(b) If the parameters are independent and there are more observations than parameters, $(A^T W A)$ will be algebraically nonsingular. However, if the chosen parameters are highly correlated with each other, $(A^T W A)$ may be very poorly conditioned and numerically singular, in the sense that the computed inverse is highly inaccurate.

(c) If the weights W_i are chosen to be the reciprocal of the variances on the corresponding C_i^{obs}, then the matrix $B = (A^T W A)^{-1}$ is the variance-covariance matrix for the parameter set $\Delta\vec{p}$. When the iteration procedure has converged, it follows that B for the final iteration is the variance-covariance matrix of $\vec{p}$.

(d) The variance-covariance matrix B implicitly assumes that the parametric model adopted can fit the observed counts. In so far as the observed counts are inconsistent with the assumed form of the peak, the calculated variance-covariance matrix will underestimate parameter uncertainties.

(e) Since the functional form $C(E_i,\vec{p})$ is known explicitly as a function of $\vec{p}$, the partial derivatives

$$\frac{\partial C(E_i,\vec{p})}{\partial p_j}\bigg|_{\vec{p}=\vec{p}^{(0)}}$$

can in principle be developed as explicit functions of the parameters. In practice, however, these derivatives are cumbersome algebraic expressions and are best calculated using difference ratios, i.e.,

$$\frac{\partial C(E_i,\vec{p})}{\partial p_j}\bigg|_{\vec{p}=\vec{p}^{(0)}} = \frac{C(E_i, p_k^{(0)} + \Delta\delta_{kj}) - C(E_i, p_k^{(0)} - \Delta\delta_{kj})}{2\Delta} .$$

(f) If the procedure converges at all, it converges quadratically. In practice, from three to six iterations sufficed to converge from an initial $\vec{p}$ set obtained by estimating curve parameters by eye, to a final set in which L changed by less than 1 part in 10^6 on the last iteration.

(g) The parametric fit is very insensitive to the values of N_1 and N_2. After some initial experimentation, these values were fixed at 20 and 40, respectively, for practical peak fitting. The model thus became effectively a nine-parameter model.

The quantity of physical interest is the area under the peak, rather than the parameter set $\vec{p}$ defining its detailed shape. This area is readily obtained, being simply

$$A = \sum_{i=1}^{I} C(E_i,\vec{p}') ,$$

where $\vec{p}'$ is the final vector of parameters obtained from the least-squares fit, but with the elastic radiative tail subtracted out, i.e., with $a = b = c = 0$. Thus $\vec{p}' \equiv (0, 0, 0, \alpha, E_{\text{inel}}, E_M, d, N_1, S_1, S_2)$.

We also need the variance on A. This is readily found, being given by

$$\mu(A) = (\sigma[A])^2 = \sum_{i=1}^{I}\sum_{k=1}^{I} (A'B'A'^T)_{ik} ,$$

where A' and B' are the matrices A and B with the rows and columns corresponding to parameters a, b, and c deleted.

Note that the area under the peak is correctly obtained by *summing* the functional form $C(E,\vec{p}')$ evaluated at each energy E_i in the energy range,

rather than by integrating it over the energy range. This is consistent with the fact that the observed counts C_i to which the fit is made already represent integrals over energy ranges $(E_i - \Delta E,\ E_i + \Delta E)$. The fit is therefore to a histogram rather than to a continuous energy spectrum.

APPENDIX B

For completeness, the kinematical relations leading to the Jacobian of solid angles are written down here.[36] The two-body final state for the reaction

$$m_1 + m_2 \rightarrow m_3 + m_4 \tag{B1}$$

is transformed to a rest frame $P = (M, 0)$, i.e., $p_1 \cdot P = E_1' M$ and $p_3 \cdot P = E_3' M$ or

$$E_1' = \frac{s + m_1^2 - m_2^2}{2\sqrt{s}}, \tag{B2}$$

$$E_3' = \frac{s + m_3^2 - m_4^2}{2\sqrt{s}}, \tag{B3}$$

where the invariant

$$s = (p_1 + p_2)^2 = (p_3 + p_4)^2,$$

$$s = M^2 = m_1^2 + m_2^2 + 2m_2 E_1.$$

E_1, E_3, θ, and $d\omega$ are laboratory variables, and E_1', E_3', Θ, and $d\Omega$ are c.m. or zero-momentum variables. For the reaction $e + {}^{12}\mathrm{C} \rightarrow e' + {}^{12}\mathrm{C}^*$ let $m_1 = m_3 = m_e$, $m_2 = {}^{12}\mathrm{C}$, and $m_4 = m_2 + Q$, where $Q = 15.109$ MeV or 0 for inelastic or elastic scattering, respectively. The c.m. angle of scatter Θ is given by

$$\tan\Theta = \frac{p_3 \sin\theta}{\overline{\gamma} p_3 \cos\theta - \overline{\eta} E_3} \tag{B4}$$

with

$$E_3 = \frac{E_1 - (M_4^2 - M_2^2)/2M_2}{1 + 2E_1 \sin^2(\frac{1}{2}\theta)/M_2} \tag{B5}$$

and $\overline{\gamma} = (E_1 + m_2)/\sqrt{s}$ and $\overline{\eta} = p_1/\sqrt{s}$. Then the Jacobian of solid angles from (B4) is

$$J = \frac{d\Omega}{d\omega} = \frac{d(\cos\Theta)}{d(\cos\theta)} = \frac{\sin^3\Theta}{\sin^3\theta}\left(\overline{\gamma} - \overline{\eta}\,\frac{E_3}{p_3}\cos\theta\right). \tag{B6}$$

These are the results used in Eq. (9) where J_e, J_{inel}, $k_1'(p_1')$, q'^2, and V_T' are used. Accordingly, the reduced nuclear transition probability $B(M1, q'^2)$ is obtained in the frame with the c.m. at rest. Since the three-momentum q^2 and q'^2 differ only in the fifth decimal place in the present range of q^2, they are not distinguished in the analysis subsequent to Eq. (9).

---

*Research supported in part by the National Science Foundation Grant No. GP-16565.

[1]M. Gell-Mann, Phys. Rev. **111**, 362 (1958).

[2]Y. K. Lee, L. W. Mo, and C. S. Wu, Phys. Rev. Lett. **10**, 253 (1963); and, C. S. Wu, Rev. Mod. Phys. **36**, 618 (1964).

[3]D. H. Wilkinson, Phys. Lett. **31B**, 447 (1970).

[4]J. Blomquist, Phys. Lett. **35B**, 375 (1971).

[5]J. S. O'Connell, T. W. Donnelly, and J. D. Walecka, Phys. Rev. **C6**, 716 (1972).

[6]L. L. Foldy and J. D. Walecka, Phys. Rev. **140**, B1339 (1965).

[7]B. T. Chertok, Phys. Rev. **187**, 1340 (1969).

[8]F. Ajzenberg-Selove and T. Lauritsen, Nucl. Phys. **A114**, 1 (1968) in particular, p. 48, Table 12.8.

[9]E. G. Fuller, private communication.

[10]D. E. Alburger and D. H. Wilkinson, Phys. Rev. C **5**, 384 (1972).

[11]F. Gudden, Phys. Lett. **10**, 313 (1964).

[12]J. C. Bergstrom, H. Crannell, F. J. Kline, J. T. O'Brien, J. W. Lightbody, Jr., and S. P. Fivozinsky, Phys. Rev. C **4**, 1514 (1971).

[13]S. Penner, *Experimental Techniques for Electron Scattering Investigations*, National Bureau of Standards Technical Note No. 523, 1970.

[14]J. S. Pruitt, Nucl. Instrum. Methods **92**, 285 (1970).

[15]G. A. Peterson, Phys. Lett. **25B**, 549 (1967); and private communication

[16]E. Spamer, Z. Phys. **191**, 24 (1966).

[17]B. T. Chertok and W. T. K. Johnson, Phys. Rev. Lett. **22**, 67 (1969); Phys. Rev. Lett. **22**, 265(E)(1969).

[18]Dr. J. Bergstrom and Dr. L. Cardman kindly sent us a copy of the revised computer program and some precision checks of the program, respectively.

[19]J. A. Jansen, R. Th. Peerdeman, and C. de Vries, Nucl. Phys. **A188**, 337 (1972).

[20]B. Dudelzak and R. E. Taylor, J. Phys. Radium **22**, 544 (1961).

[21]D. Dreschel, Nucl. Phys. **A113**, 665 (1968).

[22]Dr. L. Wright is acknowledged for independently checking some of the computer-generated values of f_C.

[23]D. Kurath, private communication .

[24]Dr. R. G. Arnold is gratefully acknowledged for writing a computer program to least-squares fit a linearized version of Eq. (11c).

[25]D. Kurath, Phys. Rev. **134**, B1025 (1965).

[26]J. W. Donnelly, Phys. Rev. C **1**, 833 (1970).

[27]H. W. Kuehne, P. Axel, and D. C. Sutton, Phys. Rev. **163**, 1278 (1967).

[28]L. Armstrong and C. W. Kim, Phys. Rev. C 5, 672 (1972), Refs. 2 and 8 therein.

[29]J. N. Huffaker, private communication; and C. W. Kim, private communication .

[30]R. J. Blin Stoyle and J. M. Freeman, Nucl. Phys. **A150**, 110 (1970).

[31]H. Bahcall, Nucl. Phys. **75**, 10 (1966).

[32]D. H. Wilkinson and B. E. F. Masefield, Nucl. Phys. **A158**, 110 (1970).

[33]A. Bohr and B. M. Mottelson, in *Nuclear Structure* (Benjamin, New York, 1969), Vol. I, p. 419.

[34]N. C. Mukhopadhyay and M. H. Macfarlane, Phys. Rev. Lett. **27**, 1823 (1971); Phys. Rev. Lett. **28**, 1545(E) (1972).

[35]E. Spamer, K. Gravemeyer, C. W. deJager, and L. Dieperink, in *Proceedings of the International Conference on Nuclear Electron Scattering and Photoreaction, Sendai, Japan,* edited by K. Shoda and H. Ui (Research Report of Laboratory of Nuclear Science, Tohoku University, 1972), Suppl. 2, Vol. 5, p. 419.

[36]R. Hagedorn, *Relativistic Kinematics* (Benjamin, New York, 1963). The methods developed by Hagedorn are followed here, since by working in the invariant s, they avoid the rather cumbersome approach of some earlier authors.